

# A Widely Tunable Optical Filter Using Ladder-Type Structure

S. Matsuo, Y. Yoshikuni, T. Segawa, Y. Ohiso, and H. Okamoto  
NTT Photonics Laboratories, NTT Corporation  
3-1 Morinosato Wakamiya, Atsugi, Kanagawa, Japan  
*mash@aecl.ntt.co.jp*

A novel widely tunable optical filter using ladder-type structure is proposed. This device decreases the electrode area compared with a tunable filter using an AWG. The device was fabricated using the InGaAsP-InP material system, and exhibits the tuning range of 58 nm.

**Keywords:** tunable optical filter, arrayed waveguide, MMI coupler

## Introduction

The wavelength division multiplexing (WDM) transport network has emerged as the best way to realize the flexible large-capacity network needed for future Internet traffic. For example, in Local Area Networks (LANs), there is a demand for transmitting a large capacity data in a few moments. When WDM technologies used, a large-capacity network using tunable optical filters can be constructed inexpensively because the network has flexible connections. In such networks, widely tunable optical filters are needed because coarse-WDM is usually used in the LANs, WANs, and SANs.

A tunable filter using an arrayed waveguide grating (AWG) has already been developed using the polymer waveguide [1,2]. That device has a tuning range of more than 30 nm. It has the electrodes for changing the refractive index on each waveguide in the array and the length of each electrode successively increases by the same length. This type of tunable filter could feasibly achieve a tunable range of more than 100 nm because the tuning range is determined by the electrode length on waveguide array and there is no theoretical limitation on the electrode length. However, the problem is that this device needs a large electrode area because the length of each electrode on the waveguide array increases successively.

In this letter, we propose a novel tunable filter using a ladder-type structure that uses multiple MMI couplers and a waveguide array. The electrodes are on the input and output waveguides and increasing the length of the electrodes is unnecessary. Thus, the electrode area is smaller than that of the previously reported device using the AWG. The device was fabricated using the InGaAsP-InP material system, and exhibits a wide tuning range of 58 nm.

## Device structure and design

Figure 1 shows a schematic diagram of the proposed tunable filter using the ladder-type structure. The device consists of input and output waveguides, the waveguide array, and optical couplers. Each arrayed waveguide is connected to the input and output waveguides by optical couplers. The interference between the lights from output and arrayed waveguide occurs at every optical coupler of the output waveguide. When the length of the waveguides is increased one after another by  $\Delta S$  as shown in Fig. 1 and the distances between the optical couplers in input and output waveguides,  $L_1$  and  $L_2$ , are the same, the resonant wavelength in every optical coupler of the output waveguide is the same. Then the resonant wavelength of this filter,  $\lambda_0$ , is given by

$$\lambda_0 = \frac{n_{eff}\Delta S}{m} \quad (1)$$

where  $n_{eff}$  is the effective refractive index of a waveguide and  $m$  is the diffraction order.

When the refractive index in the input waveguide is decreased, the optical path length difference between the optical path from the output and arrayed waveguides is decreased. Therefore, the resonant wavelength change,  $\Delta\lambda$ , is given by

$$\Delta\lambda = \frac{\Delta n_{eff} L_1}{m} \quad (2)$$

where  $\Delta n_{eff}$  is the effective refractive index change in the input waveguide. On the other hand, when the refractive index is decreased in output waveguide, the optical path length difference is increased. Thus the resonant wavelength shifts for longer wavelength when the refractive index is increased. Note that the length of waveguide for refractive index change is no limitation as shown in eq. (1). Thus, this device has capability for wide range tuning.

The total tuning electrode length of the input waveguide in proposed device,  $L_{propose}$ , is given by

$$L_{propose} = (N-1)L_1 \quad (3)$$

where  $N$  is number of arrayed waveguides. On the other hand, the total tuning electrode length of the device in Ref [2] to obtain the same tuning range with proposed device,  $L_{AWG}$ , is given by,

$$L_{AWG} = \frac{N(N-1)}{2} L_1 . \quad (4)$$

Thus, the total length of the tuning electrode is improved by

$$\frac{L_{propose}}{L_{AWG}} = \frac{(N-1)L_1}{N(N-1)L_1/2} = \frac{2}{N} . \quad (5)$$

It seems that the proposed device would have low power consumption and high yield.

Figure 2 shows the calculated input-output characteristics of the proposed device as a function of arrayed waveguide number. In this calculation, we assumed that the diffraction order,  $m$ , was 20. We use an MMI coupler as an optical coupler because it is suitable for use with the high-mesa waveguide structure. We assumed the splitting ratio of the MMI coupler was 0.15 in power. This value is the smallest value for a simple MMI structure [3]. As shown in this figure, the 3-dB bandwidth decreases from 7.0 to 3.6 nm with increasing arrayed waveguide number. The loss of the device, however, increased from 2.84 to 3.87 dB when the arrayed waveguide number was 20. Thus, we choose the arrayed waveguide number of 15. In this case, the loss was 2.84 dB and 3-dB bandwidth was 4.8 nm.

Figure 3 shows the calculated tuning characteristics of the proposed device. The solid line shows the frequency response without tuning and the dashed lines are frequency responses for refractive index change of -0.15 % for input and output waveguides, respectively. In this calculation, we assumed that  $L_1$  and  $L_2$  were 100  $\mu\text{m}$ , the other parameters were the same as in Fig. 2. When -0.15 %-refractive index change occurred in the input waveguide, the resonant peak decreased for 25.4 nm. When -0.15 %-refractive index change occurred in the output waveguide, the resonant peak increased for 25.4 nm. Thus, the total resonant wavelength shifts were 50.8 nm.

## Device Characteristics

Figure 4 is photograph of the fabricated tunable optical filter using the ladder-type structure. The device structure was grown by MOCVD on an n-doped InP substrate. It consists of a  $\text{p}^+$ -InGaAs contact layer, a 0.3- $\mu\text{m}$ -thick p-InP cladding layer (doping concentration of  $1 \times 10^{18} \text{ cm}^{-3}$ ), a 1.2- $\mu\text{m}$ -thick  $\text{p}^-$ -InP cladding layer (doping concentration of  $2 \times 10^{17} \text{ cm}^{-3}$ ), a 0.3- $\mu\text{m}$ -thick InGaAsP layer (1.3Q), and a 0.5- $\mu\text{m}$ -thick n-InP buffer layer. The high-mesa waveguide structure was formed by  $\text{Cl}_2$  ICP-RIE. Waveguide width and height were 1.6 and 4.0  $\mu\text{m}$ , respectively. The MMI couplers, which had the power-splitting ratio of 15:85, were 5.2- $\mu\text{m}$  wide and 56.0- $\mu\text{m}$  long. The diameter of the arrayed waveguides was 400  $\mu\text{m}$ . For current injection to change the refractive index, Ni/Zn/Au electrodes were deposited on the  $\text{p}^+$ -InGaAs contact layer. The device is 3.2 x 0.9  $\text{mm}^2$ , including the bonding pads.

Figure 5 shows the optical frequency response of the tunable filter for TE polarization. The

light source was an ASE light from a fiber amplifier. The transmissivity was normalized by the loss of the reference waveguide. This device was designed for a diffraction order of 20 and arrayed waveguide number of 15. The resonant peak was observed at 1539.5 nm and a side-lobe was also observed. The loss compared with a reference waveguide was 7.5 dB, which is larger than calculated value due to the loss of MMI couplers. The contrast ratio was 12.5 dB and 3-dB bandwidth was 4.5 nm, which agrees with calculation in Fig. 2.

Figure 6 shows the tuning characteristics of the tunable filter. There was no injection current, and two-resonant wavelengths were observed at 1534.6 and 1609.0 nm. Thus, the FSR of this device was 74.4 nm. The injection current of the input waveguide was changed from 0 to 30 mA, while that of the output waveguide was kept constant at 0 mA. The refractive index in input waveguide decreased with increasing injection current. Thus, the resonant wavelength of the filter gradually decreased. The resonant wavelength shift was 29 nm at injection current of 30 mA. When the injection current of the output waveguide was changed from 0 to 30 mA, the resonant wavelength increased by 29 nm. Thus, the total tunable range is 58 nm. As described before, increasing the length of the current injection area could be the reason for the increased tunable range.

### **Conclusion**

We have proposed and demonstrated a widely tunable optical ladder-type filter that uses the multiple MMI couplers and a waveguide array. The device shows loss, compared with a reference waveguide, of 7.5 dB. The contrast ratio is 12.5 dB and the 3-dB bandwidth is 4.5 nm. These values are consistent with the calculation results. The total tuning range is 58 nm.

### **Acknowledgement**

We thank J. Yumoto and C. Amano for helpful discussions and T. Kodaira and K. Ishibashi for device fabrication and measurements.

### **References**

- [1] T. Watanabe, Y. Inoue, K. Kaneko, N. Ooba, and T. Kurihara, "Polymeric arrayed-waveguide grating multiplexer with wide tuning range," *Electron. Lett.*, vol. 33, no. 18, pp. 1547-1548, 1997.
- [2] S. Toyoda, N. Ooba, K. Kitoh, T. Kurihara, and T. Maruno, "Wide tuning range and low operating power AWG-based thermo-optic wavelength tunable filter using polymer waveguide," *Electron. Lett.*, vol. 37, no. 18, pp. 1130-1132, 2001.
- [3] M. Bachmann, P.A. Besse, and H. Melchior, "Overlapping-image multimode interference couplers with a reduces number of self-images for uniform and nonuniform power splitting," *Appl. Optics*, vol. 34, no. 30, pp.6898-6910, 1995.

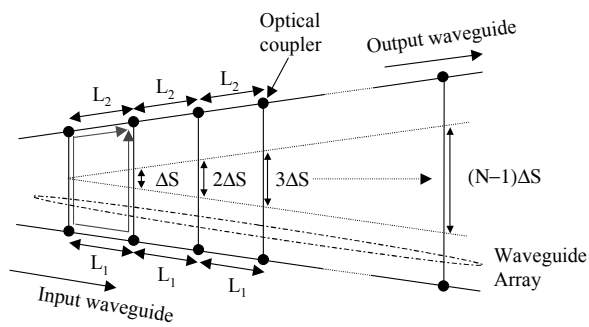


Fig. 1 Schematic diagram of the proposed device.

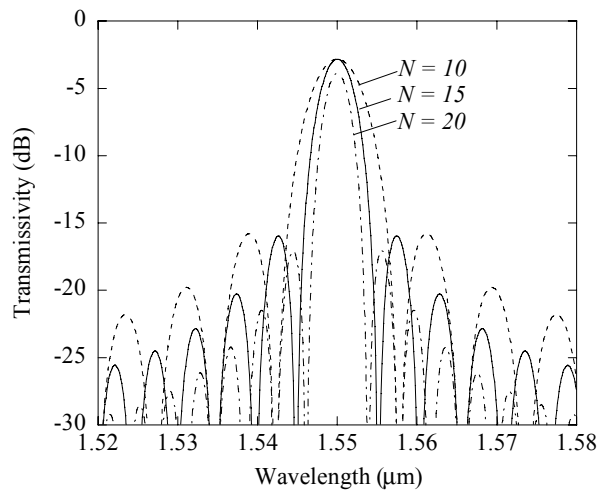


Fig. 2 Calculated input-output characteristics as a function of waveguide number.

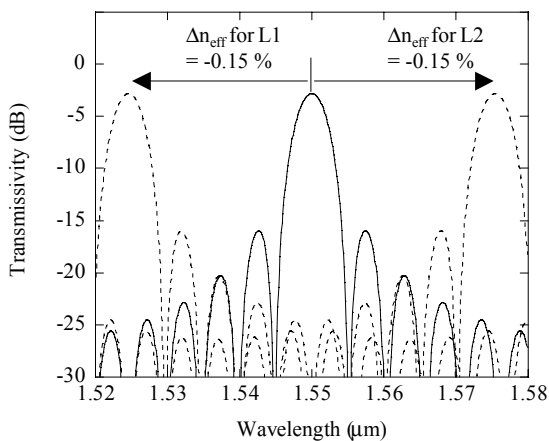


Fig. 3 Calculated tuning characteristics.

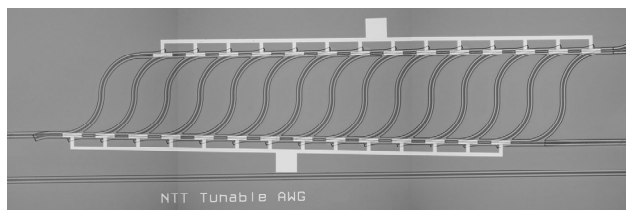


Fig. 4 Photograph of the device.

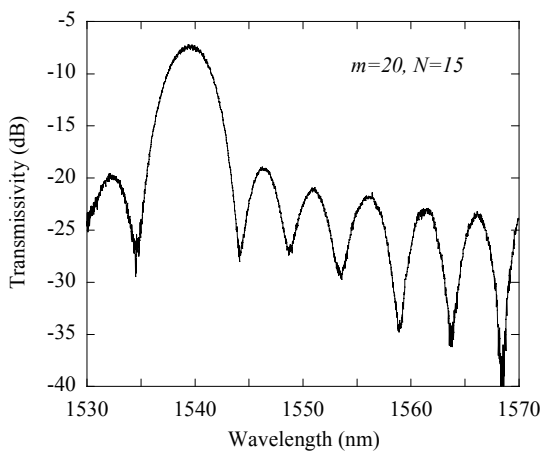


Fig. 5 Input-output characteristics of the device.

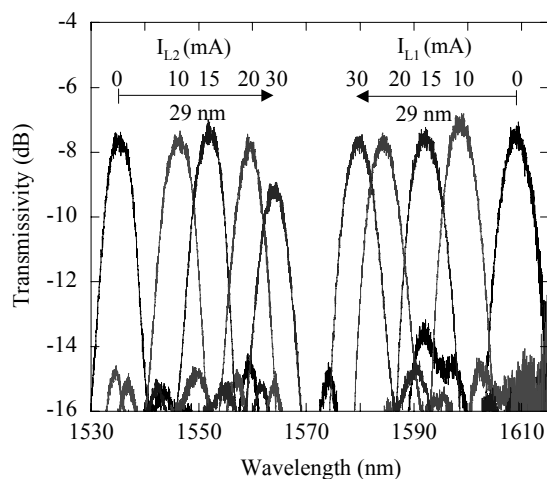


Fig. 6. Tuning characteristics of the device.